SUPPLEMENTARY INFORMATION

An engineered Axl 'decoy receptor' effectively silences the Gas6/Axl signaling axis

Mihalis S. Kariolis[1], Yu Rebecca Miao[2], Douglas S. Jones II[1], Shiven Kapur[1], Irimpan I. Mathews[3], Amato J. Giaccia[2*], Jennifer R. Cochran[1*]

[1] Department of Bioengineering, Stanford University, Stanford, California 94305, USA

[2] Department of Radiation Oncology, Stanford University School of Medicine, Stanford University, Stanford, California 94305, USA

[3] Stanford Synchrotron Radiation Lightsource, SLAC National Accelerator Laboratory, 2575 Sand Hill Road MS 99, Menlo Park, California 95124, USA

[*]Co-corresponding author

Supplementary Results

Supplementary Figures

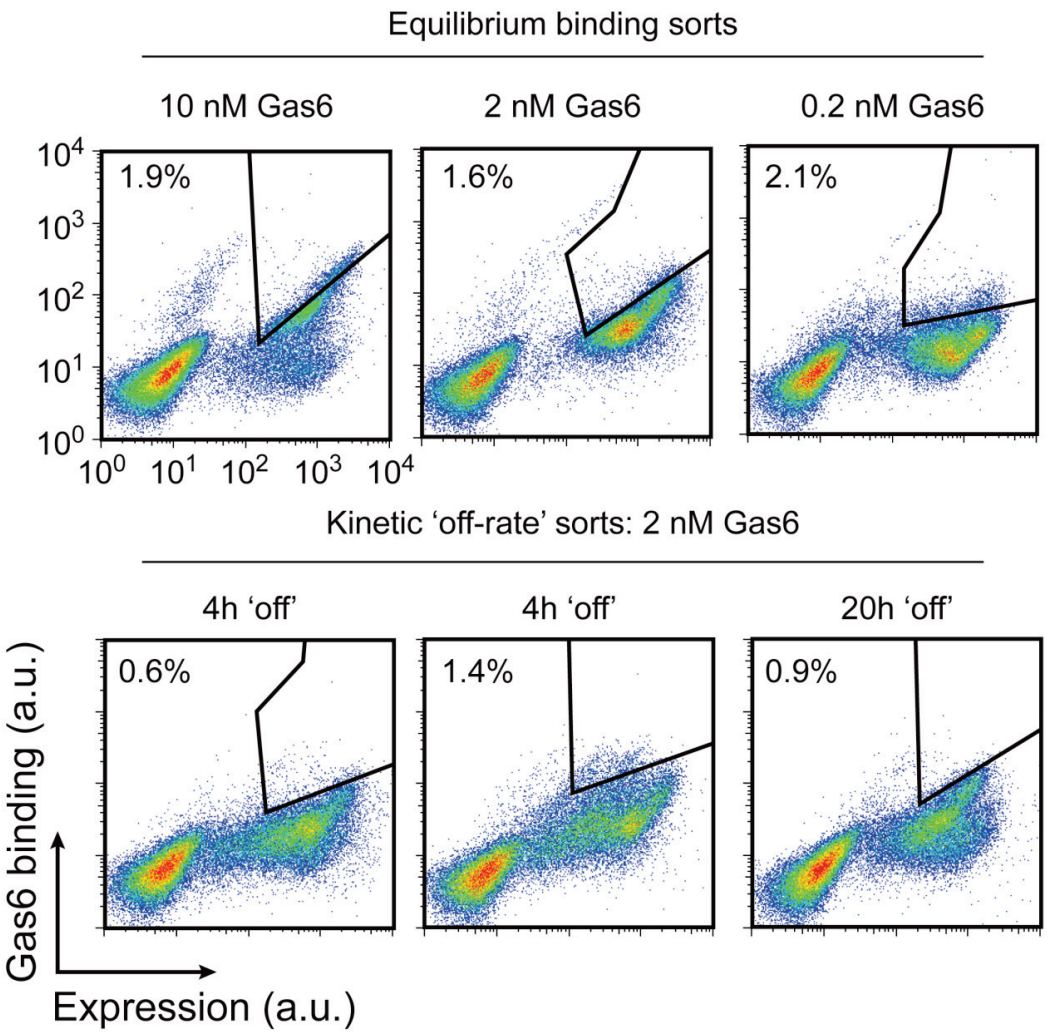

Supplementary Figure 1: Flow cytometry dot plots showing sort gates and conditions used for Axl library screen. The first three sorting rounds were performed under equilibrium binding conditions. Screening stringency was imparted by decreasing the amount of Gas6 incubated with the library in each successive round of sorting. In the final three sorting rounds, the library was screened based on kinetic off-rate sort parameters in which high-affinity clones were isolated based on their ability to retain binding to Gas6 after incubation with excess competitor. Percentages in each panel correspond to the subpopulation collected, see Methods for additional details.

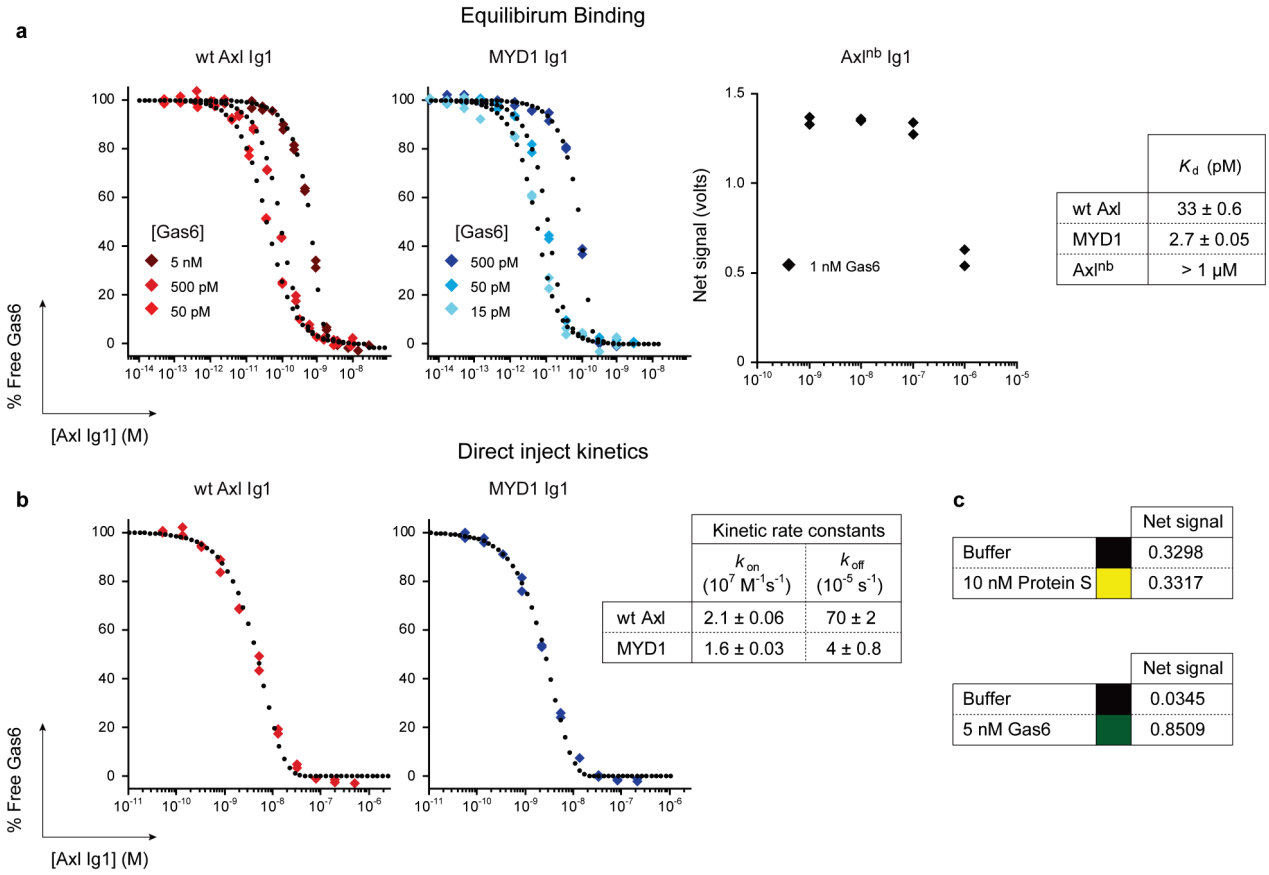

	K_d (pM)
wt Axl	33 ± 0.6
MYD1	2.7 ± 0.05
Axl^{nb}	> 1 µM

	Kinetic rate constants	
	k_{on} (10^7 $M^{-1}s^{-1}$)	k_{off} (10^{-5} s^{-1})
wt Axl	2.1 ± 0.06	70 ± 2
MYD1	1.6 ± 0.03	4 ± 0.8

c

	Net signal
Buffer	0.3298
10 nM Protein S	0.3317

	Net signal
Buffer	0.0345
5 nM Gas6	0.8509

Supplementary Figure 2: KinExA measurements of Axl Ig1 variants. (**a**) N-curve analysis of Gas6 binding titrations for wild-type Axl Ig1, MYD1 Ig1, and Axl^{nb} Ig1. N-curve analysis of Axl^{nb} could not be performed as complete binding to 1 nM of Gas6 was not attained even at μM concentrations of Axl^{nb}. This corresponds to a $K_d > 1\mu M$ which is out of the measurable range of this assay. (**b**) KinExA direct inject kinetic data for wild-type Axl Ig1 and MYD1 Ig1. (**c**) KinExA signal tests of Protein S and Gas6 binding to MYD1 Fc coated beads. MYD1 Fc does not bind Protein S as no signal was detected after 700 μl of a 10 nM Protein S solution was passed over beads (left). In comparison, a robust signal was obtained after 100 μl of a 5 nM solution of Gas6 was flowed over the same beads. Curve fits are shown as dotted black lines and nominal concentrations of Gas6 are indicated.

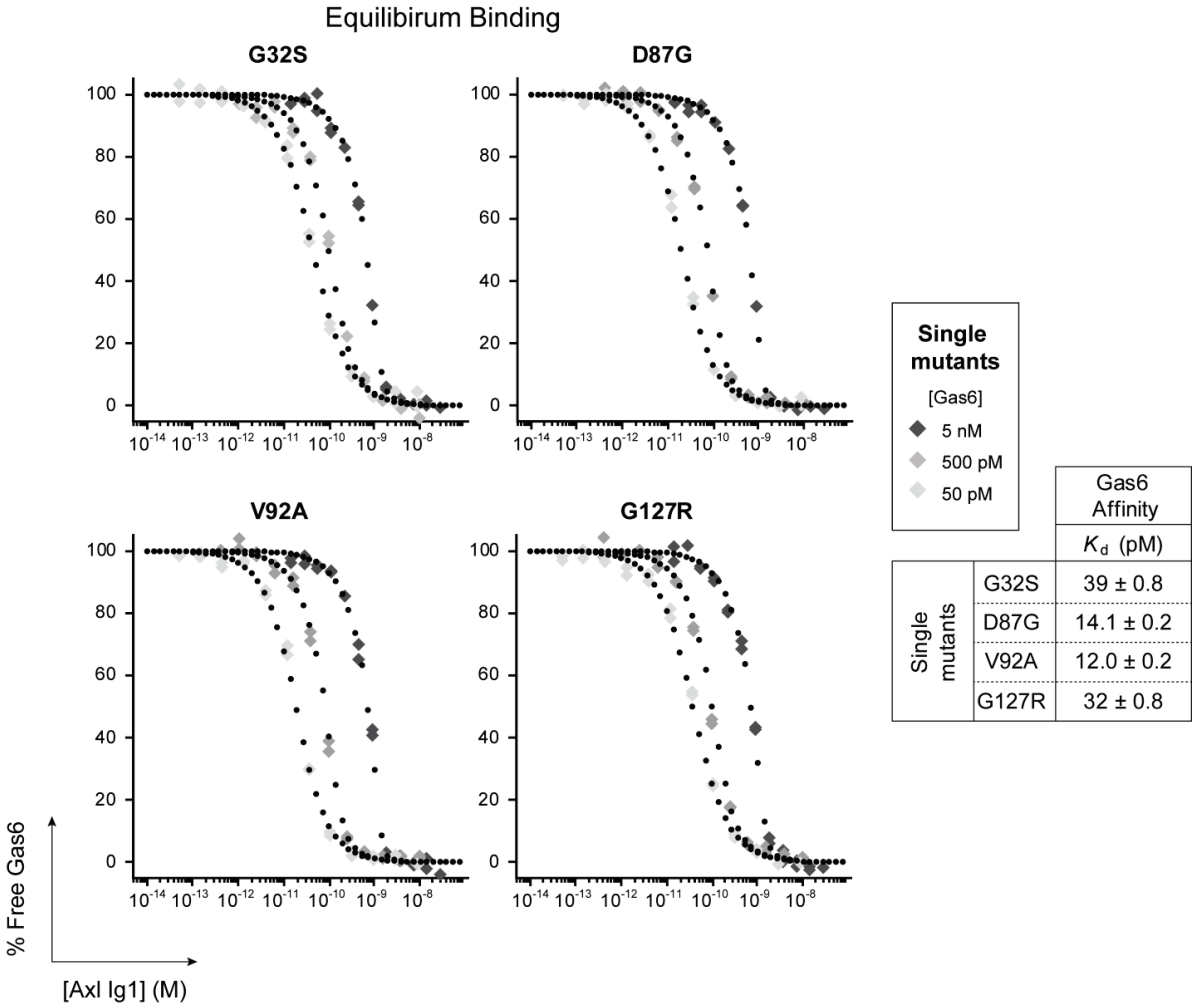

		Gas6 Affinity
		K_d (pM)
Single mutants	G32S	39 ± 0.8
	D87G	14.1 ± 0.2
	V92A	12.0 ± 0.2
	G127R	32 ± 0.8

Supplementary Figure 3: KinExA measurements of MYD1 Ig1 single point mutants. N-curve analysis was performed using binding titrations to 5 nM, 500 pM, and 50 pM of Gas6 for each single mutant of MYD1 to determine the binding affinity values shown in **Fig. 1e**. Curve fits are shown as dotted black lines and nominal concentrations of Gas6 are indicated.

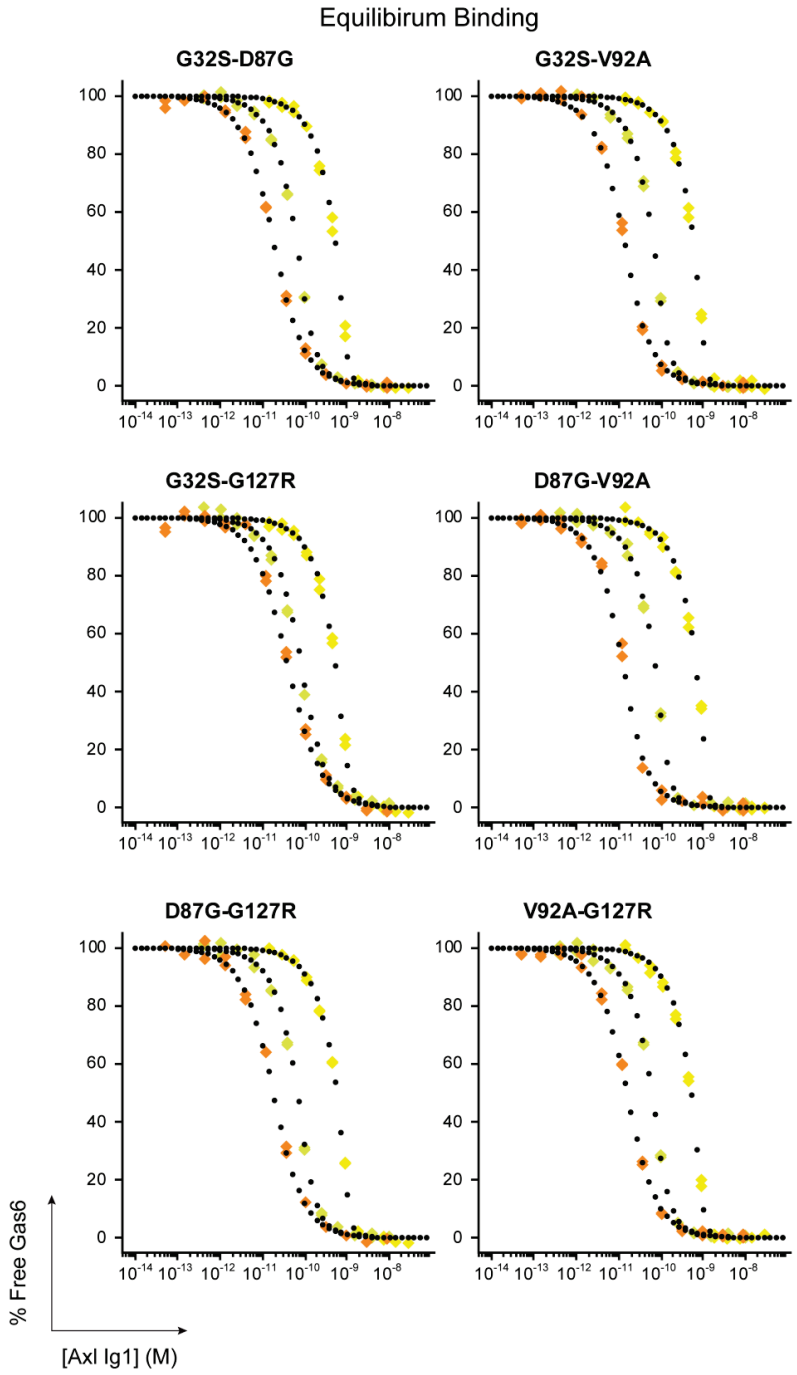

Double mutants	Gas6 Affinity K_d (pM)
G32S-D87G	13.5 ± 0.2
G32S-V92A	7.9 ± 0.1
G32S-G127R	35.0 ± 0.7
D87G-G127R	12.8 ± 0.2
V92A-G127R	10.9 ± 0.2
D87G-V92A	5.7 ± 0.1

Supplementary Figure 4: KinExA measurements of MYD1 Ig1 double point mutants. N-curve analysis was performed using binding titrations to 5 nM, 500 pM, and 50 pM of Gas6 for each double mutant of MYD1 to determine the binding affinity values shown in **Fig. 1e**. Curve fits are shown as dotted black lines and nominal concentrations of Gas6 are indicated.

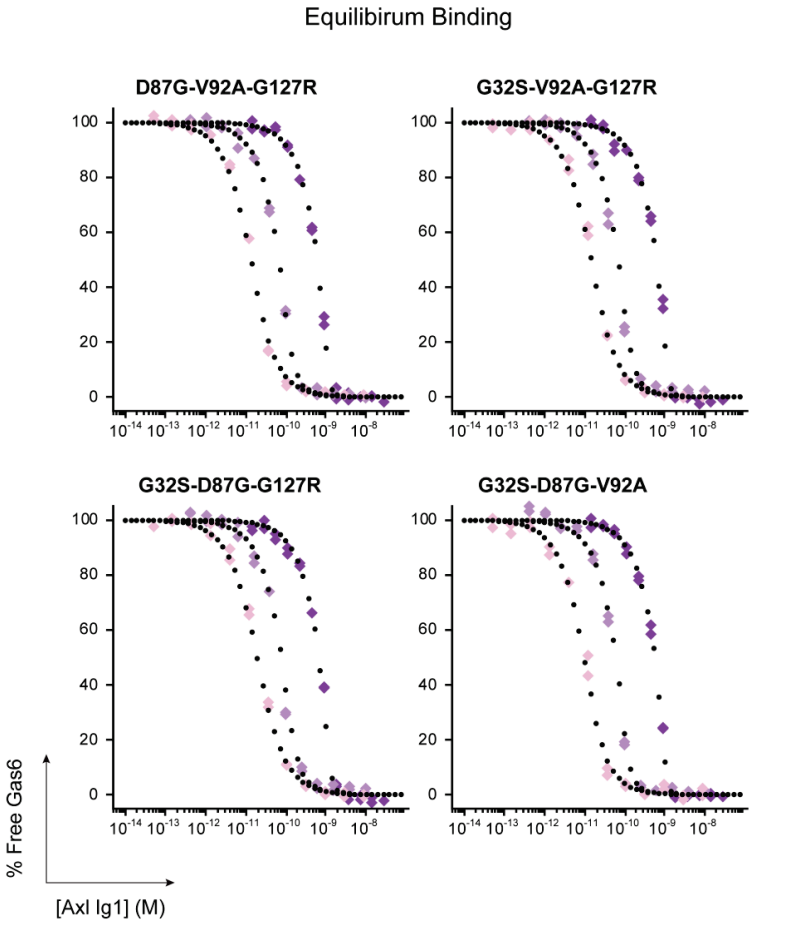

		Gas6 Affinity
		K_d (pM)
Triple mutants	D87G-V92A-G127R	7.6 ± 0.2
	G32S-V92A-G127R	8.6 ± 0.2
	G32S-D87G-G127R	13.0 ± 0.4
	G32S-D87G-V92A	4.1 ± 0.1

Supplementary Figure 5: KinExA measurements of MYD1 Ig1 triple point mutants. N-curve analysis was performed using binding titrations to 5 nM, 500 pM, and 50 pM of Gas6 for each triple mutant of MYD1 to determine the binding affinity values shown in **Fig. 1e**. Curve fits are shown as dotted black lines and nominal concentrations of Gas6 are indicated.

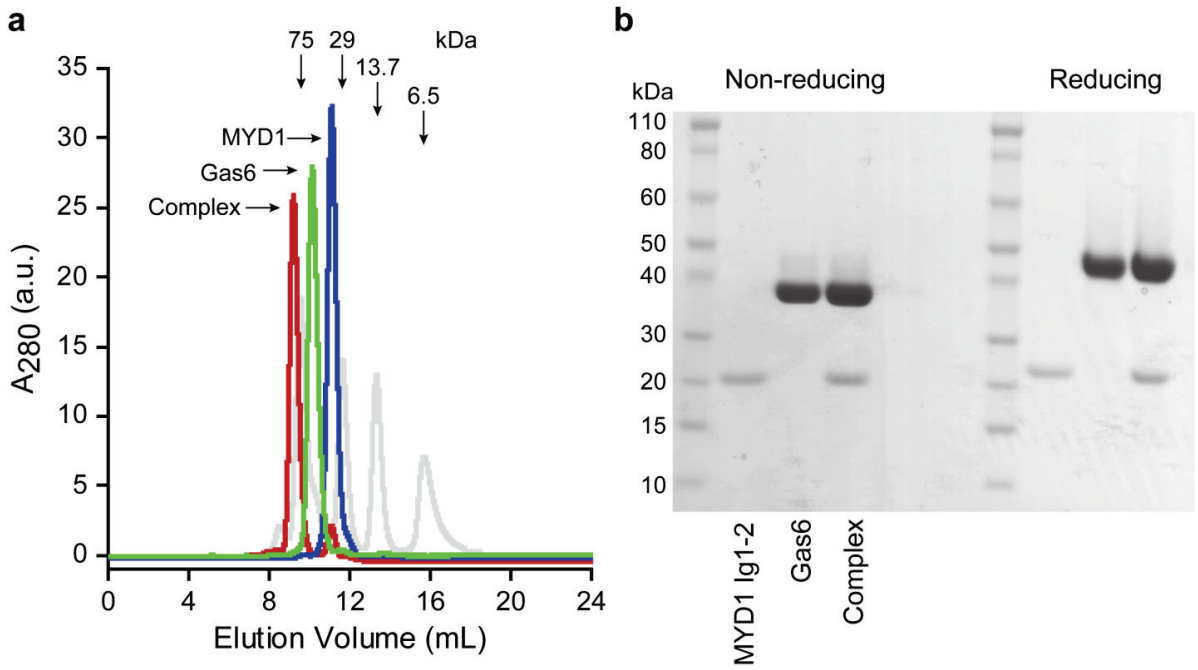

Supplementary Figure 6: Recombinant production of protein for structural studies. (**a**) Overlaid analytical size exclusion chromatography chromatograms of purified MYD1 Ig1-2, Gas6, and the Gas6/MYD1 co-complex. The increased molecular weight of the co-complex resulted in a decreased retention time on the column allowing the unbound MYD1 Ig1-2 (small peak) to be removed. (**b**) SDS-PAGE of purified MYD1 Ig1-2, Gas6, and co-complex demonstrates the complex was appropriately forming between Gas6 and MYD1 and was not the result of homo-oligomerization of either protein. Lanes on the reducing gel are the same as indicated on the non-reducing gel.

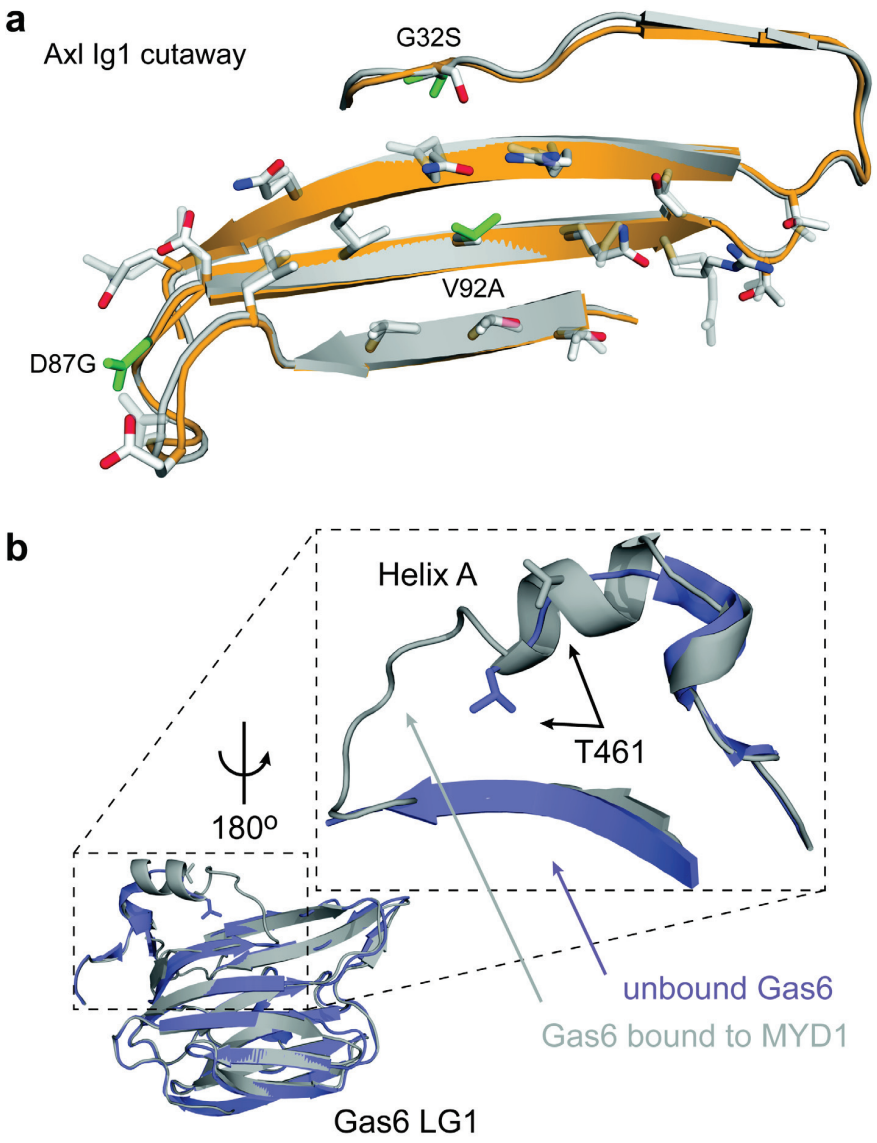

Supplementary Figure 7: Structural reorganization upon MYD1/Gas6 binding. (**a**) Cutaway of the front side of MYD1 Ig1, which contacts Helix A on Gas6. MYD1 is shown in orange, with wild-type Axl overlaid in transparent gray. Side chains that have significantly different conformations in the two structures are shown, with the mutated wild-type residues highlighted in green. (**b**) Ribbon model of Gas6 LG1 structures when unbound (purple, PDB ID 1H30) and when bound to MYD1 (gray). The loop following strand L is disordered and not resolved in the Gas6 structure, but forms a short α-helix upon binding to MYD1. For reference, the side chain of T457 is shown in sticks in both structures. Structuring of this loop upon engagement with MYD1 is consistent with that observed for binding to wild-type Axl[25].

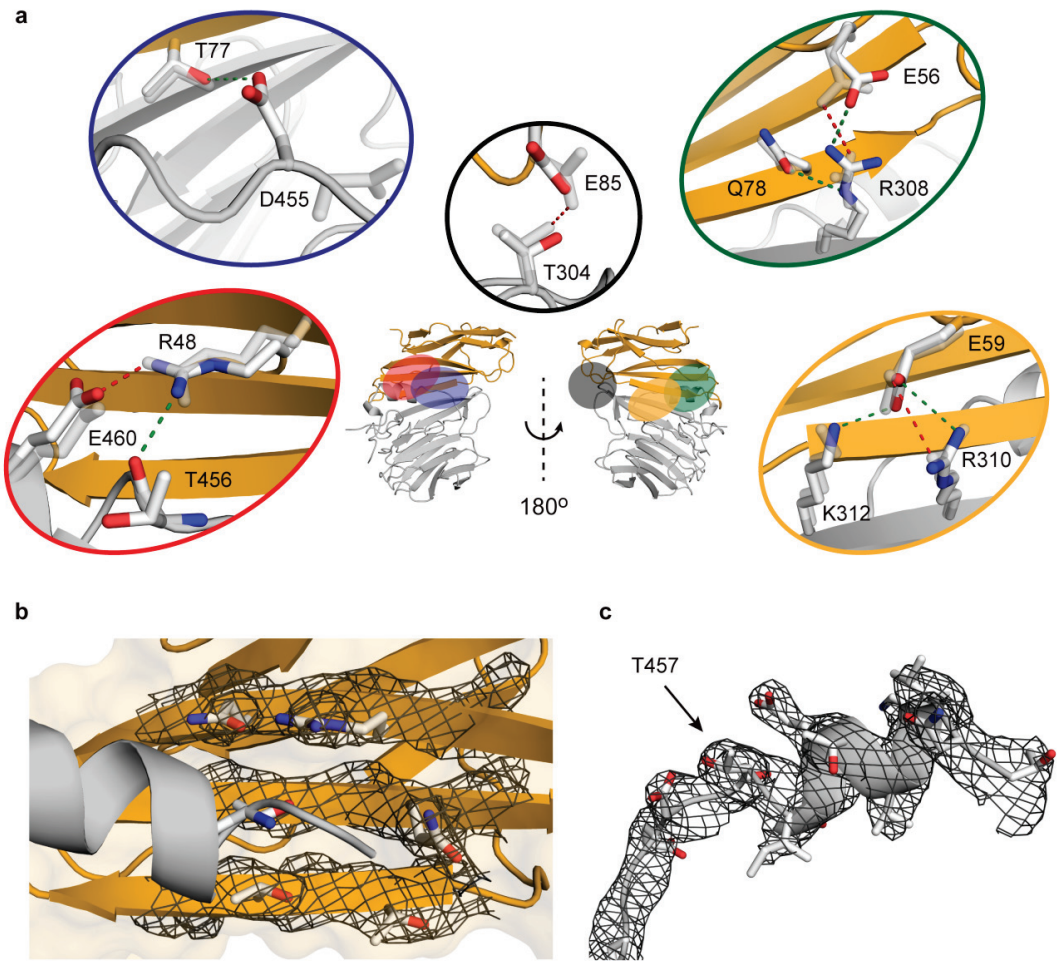

Supplementary Figure 8: Structural basis of high-affinity Gas6/Axl binding. (**a**) Side chain interactions gained (green dashes) and lost (red dashes) in Gas6/MYD1 complex compared to the wild-type complex (PDB ID 2C5D). Wild-type side chains are overlaid in transparent gray for comparison. The color of outlined ovals matches the shaded patches on the ribbon model (center) to indicate the location of each highlighted region. (**b**) The electron density map is overlaid on the Gas6/MYD1 co-complex to demonstrate the resolution of the data at positions that were found to participate in the new groove on MYD1 (**b**) and Helix A (**c**) on Gas6. The $2F_o - F_c$ map is contoured at 1.5 σ. See **Supplementary Table 6** for additional technical information on R308 and R310.

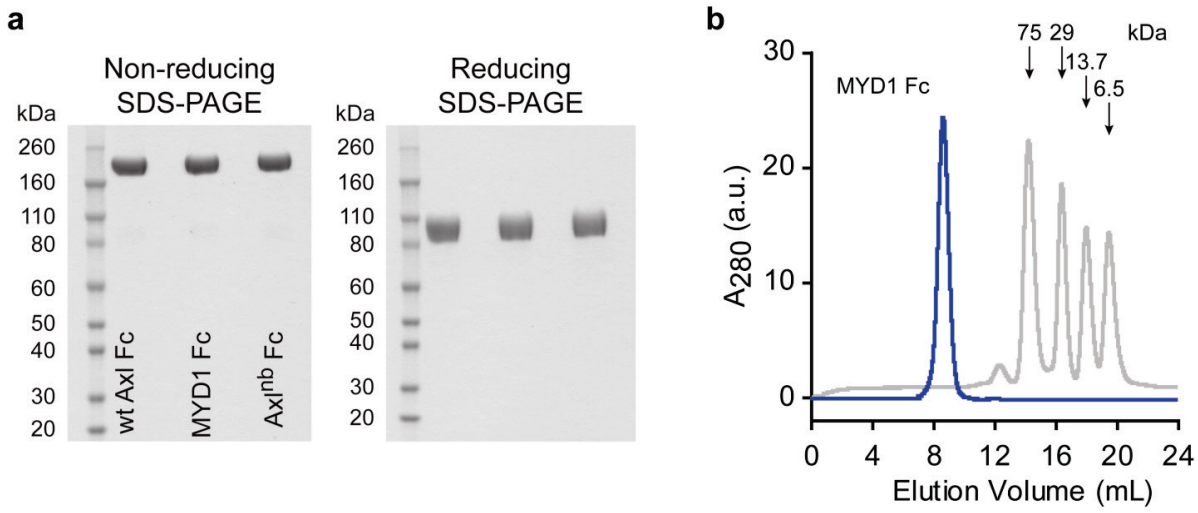

Supplementary Figure 9: SDS-PAGE and analytical size exclusion chromatography of purified Axl Fc fusions. (**a**) SDS-PAGE of full-length Axl Fc fusions. The molecular weight of the protein is halved under reducing conditions, verifying the proper formation of the disulfide-linked homodimer. Lanes on the reducing gel are the same as indicated in the non-reducing gel. (**b**) Analytical size exclusion chromatography chromatogram for 25 µg of MYD1 Fc.

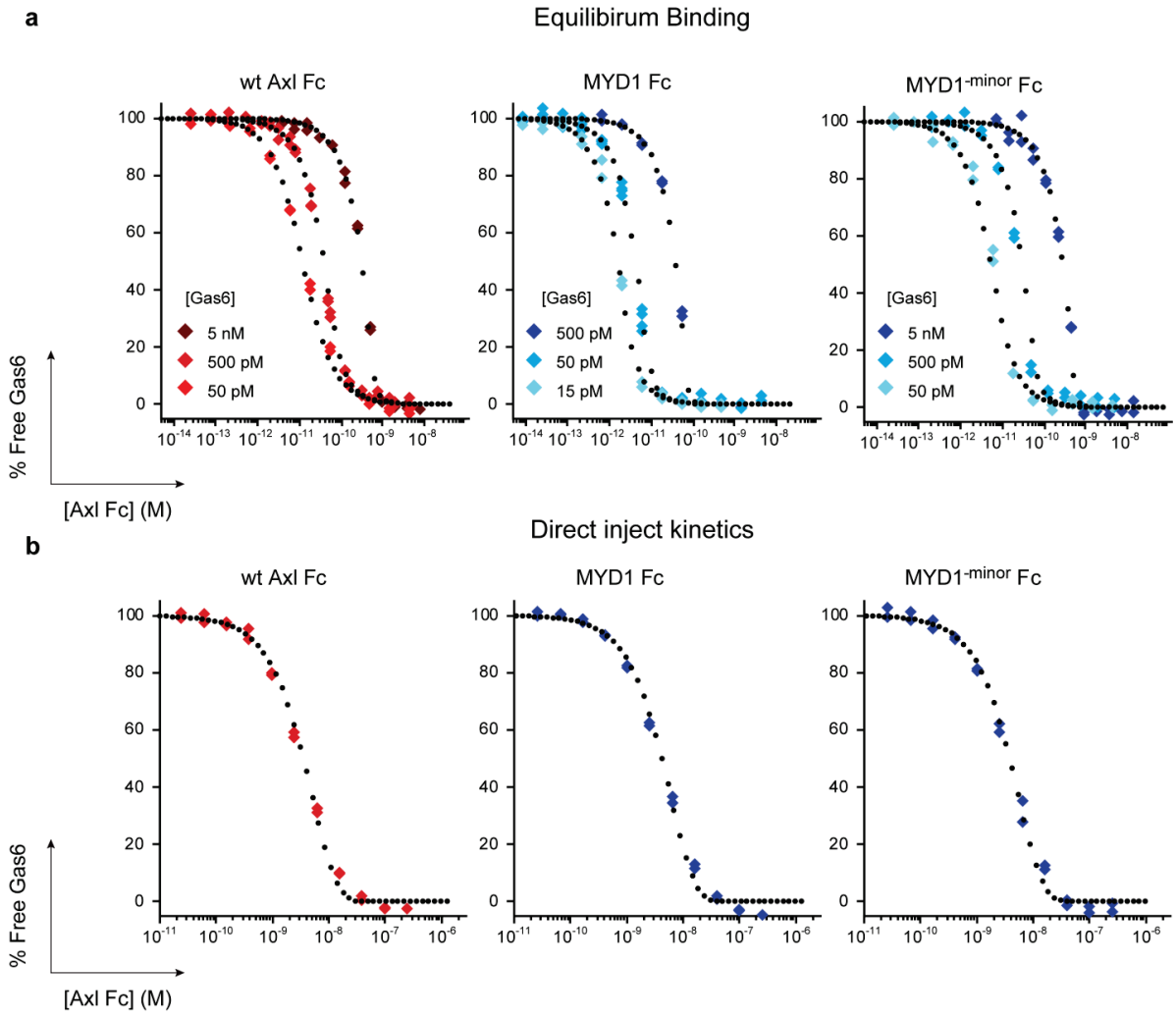

	K_d (fM) (apparent)
wt Axl Fc	9,200 ± 200
MYD1 Fc	420 ± 10
MYD1^{-minor} Fc	2,600 ± 100
MYD1 Ig1 Fc	1,700 ± 30
MYD1 Ig1-2 Fc	2,600 ± 50

	Kinetic rate constants	
	k_{on} (10^7 $M^{-1}s^{-1}$)	k_{off} (10^{-5} s^{-1})
wt Axl Fc	2.6 ± 0.07	24 ± 0.07
MYD1 Fc	2.3 ± 0.06	1.0 ± 0.02
MYD1^{-minor} Fc	2.5 ± 0.08	6.7 ± 0.2
MYD1 Ig1 Fc	n.d.	n.d.
MYD1 Ig1-2 Fc	2.7 ± 0.06	7.0 ± 0.2

Supplementary Figure 10: Binding affinity measurements of Axl Fc fusions. (**a**) N-curve analysis to determine binding affinity of Gas6 to wild-type Axl, MYD1 and MYD1^{-minor} Fc fusions. (**b**) Direct inject kinetic data to determine the k_{on} of binding interactions. Curve fits are shown as dotted black lines and nominal concentrations of Gas6 are indicated.

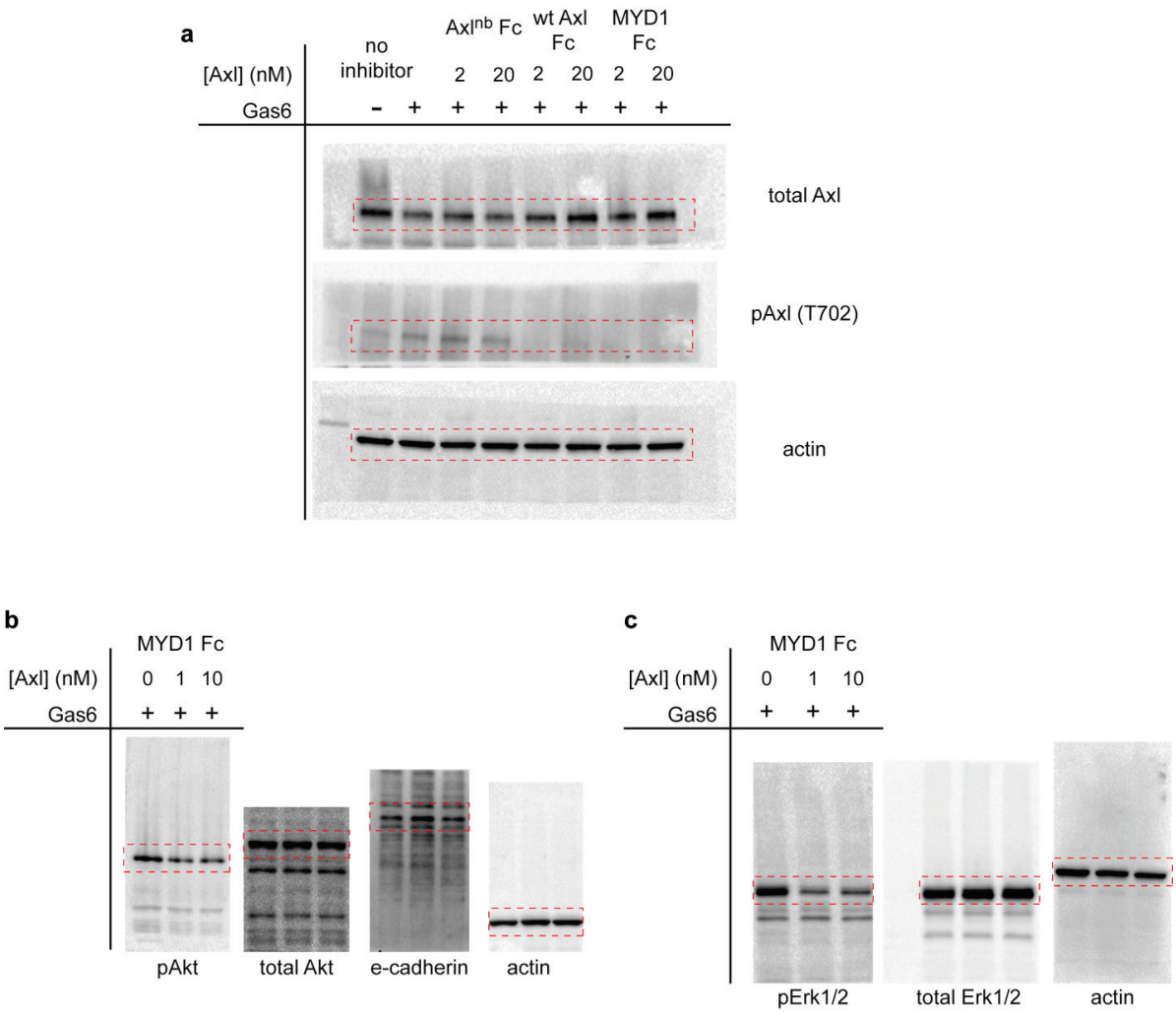

Supplementary Figure 11: Uncropped western blots from Fig. 4 (**a**) Wild-type Axl Fc and MYD1 Fc, but not Axl^{nb} Fc, can inhibit Gas6-mediated Axl activation *in vitro*. (**b**) and (**c**) Inhibition of Axl activation leads to reduced levels of phosphorylated Akt and Erk1/2, and an increase in the epithelial marker e-cadherin. Red boxes indicated regions cropped for display in Figure 4.

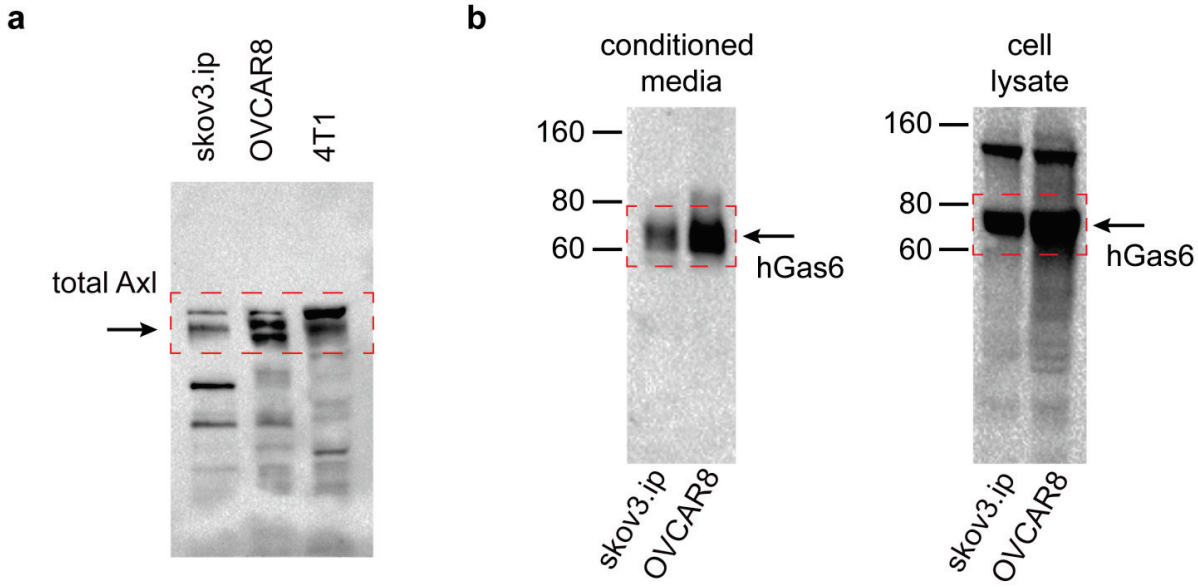

Supplementary Figure 12: Western blot analysis of Axl and Gas6 expression. (**a**) High Axl expression is observed on each of the three cell lines used in this study. (**b**) Both human ovarian cancer cell lines have autocrine Gas6 production.

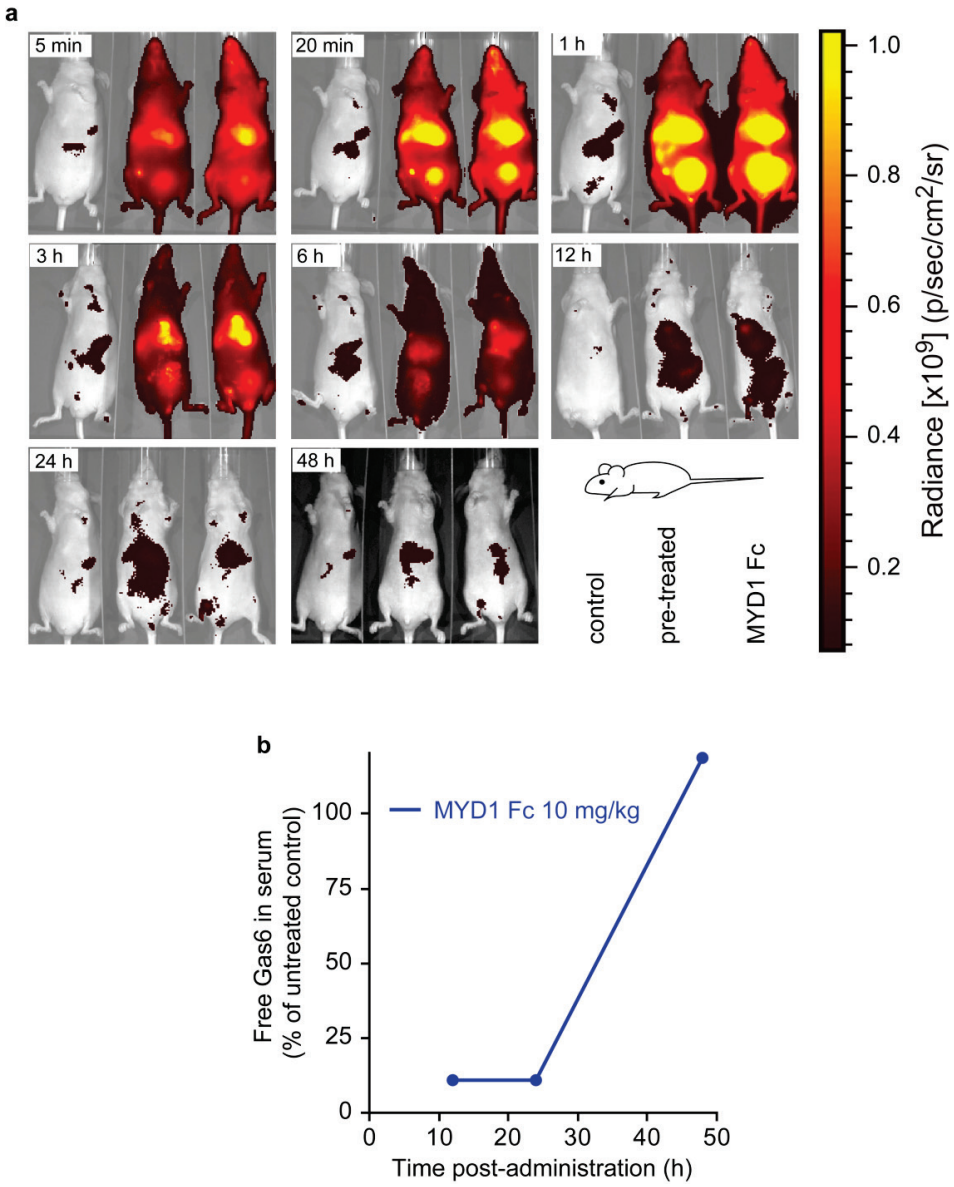

Supplementary Figure 13: Whole body optical imaging of fluorescently labeled MYD1 Fc. (**a**) Whole body near-infrared optical imaging was performed on mice after administration of a single 1 mg/kg dose of Alexa Fluor 680 labeled MYD1 Fc. Mice were given one of three injections: saline (left), two 10 mg/kg predoses of unlabeled MYD1 Fc, one on each of the two days preceding the imaging study, and a single labeled dose of MYD1 Fc the day of the study (middle), or a single dose of labeled MYD1 Fc (right). (**b**) Free serum Gas6 following a single 10 mg/kg dose of MYD1 Fc illustrating complete removal of Gas6 for up to 24 hours. This indicates that no Gas6 was present in the predosed mouse at the start of the imaging study.

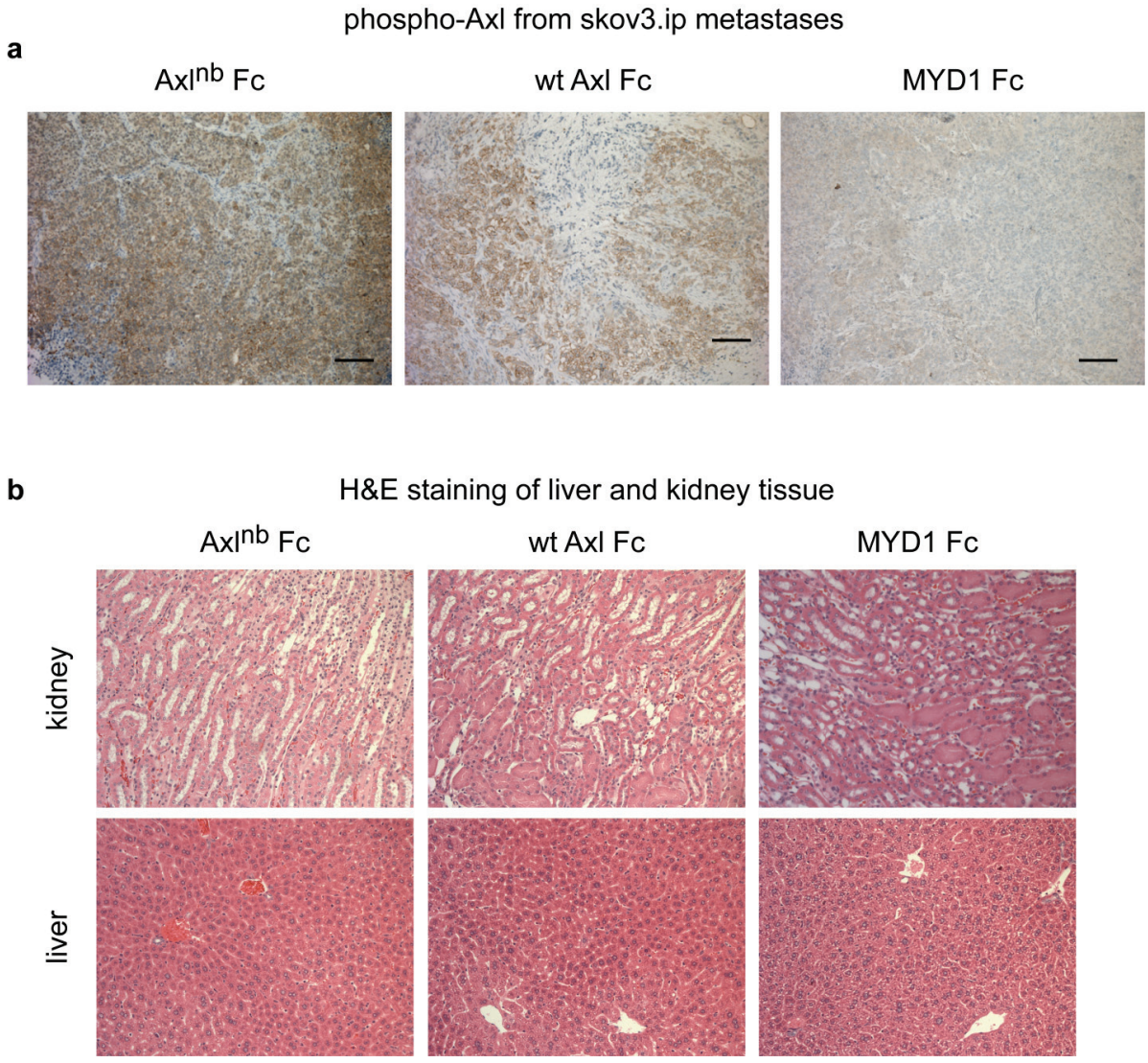

Supplementary Figure 14: MYD1 Fc is well-tolerated and inhibits Axl signaling in vivo. (**a**) Immunohistochemical staining of phosphorylated Axl in tumor tissue taken from mice from the skov3.ip study. Images are 20X magnification of representative tissue slices. Bars are 50 μM (**b**) Representative H&E staining of liver and kidney tissue indicating that the Axl decoy receptors do not elicit significant cellular toxicity.

SUPPLEMENTARY TABLES

Supplementary Table 1: Sequences of clones randomly sequenced from sort 5 products

Twenty-three clones were sequenced at random from the pool of Axl mutants recovered from sort 5, revealing ten unique sequences. The number of amino acid mutations in each clone, what those mutations were relative to the wild-type residue, and the frequency of each clone are indicated. Note the emergence of the V92A consensus mutation.

Clone	AA	19	26	27	32	72	79	86	87	90	92	127	# of repeats
wt Axl		A	E	E	G	A	V	Q	D	I	V	E	
1	4		G				M				A	E	2
2	1								G				1
3	1										A		3
4	4				S				G		A	R	7
5	2							R			A		1
6	1					V							3
7	4	T	G	G							A		1
8	2									M	A		1
9	1										G		2
10	3							R		V	A		1
											Total:		23

Supplementary Table 2: Sequences of clones randomly sequenced from sort 6 products

Fifteen clones were sequenced at random from the pool of Axl mutants recovered from sort 6, revealing three unique sequences. The number of amino acid mutations in each clone, what those mutations were relative to the wild-type residue, and the frequency of each clone are indicated. Two clones, MYD1 and MYD2, dominate the remaining pool and all sequences contain the V92A mutation.

Clone	AA	26	32	33	74	79	87	92	127	# of repeats
wt Axl		E	G	N	S	V	D	V	G	
MYD1	4		S				G	A	R	9
MYD2	4	G				M		A	E	5
MYD3	4			S	N		G	A		1
								Total:		15

Supplementary Table 3: Calculated changes in the free energy of binding of Axl Ig1 variants

	Residue no. 32	87	92	127	ΔG° (kcal/mol)	$\Delta\Delta G^{\circ}$ to wt Axl
wt Axl	G	D	V	G	-14.29	- - -
MYD1	S	G	A	R	-15.77	-1.48
Single mutants	S				-14.19	0.10
		G			-14.79	-0.50
			A		-14.89	-0.60
				R	-14.31	-0.01
Double mutants	S	G			-14.82	-0.53
	S		A		-15.14	-0.84
	S			R	-14.26	0.04
		G		R	-14.85	-0.56
			A	R	-14.95	-0.65
		G	A		-15.33	-1.04
Triple mutants		G	A	R	-15.16	-0.87
	S		A	R	-15.09	-0.79
	S	G		R	-14.84	-0.54
	S	G	A		-15.53	-1.23

Supplementary Table 4: Thermal stabilities of Axl Ig1 variants as measured by circular dichroism temperature melts

	Residue no. 32	87	92	127	T_m (°C)
wt Axl	G	D	V	G	53 ± 0.6
MYD1	S	G	A	R	54 ± 0.9
Single mutants	S				52 ± 0.6
		G			55 ± 0.4
			A		47 ± 1.0
				R	57 ± 0.4

Supplementary Table 5: Crystallographic parameters

Data Collection	**Gas6/MYD1**
Space group	$P3_221$
Cell dimensions	
a, b, c (Å)	112.37, 112.37, 361.26
α, β, γ (°)	90, 90, 120
Resolution (Å)	38.01 – 3.07(3.15)*
R_{sym}[a] (%)	11.8 (100.0)
I/σ	20.4 (2.1)
Completeness (%)	99.9 (100)
Redundancy	11.9 (7.1)
Refinement statistics	
Resolution (Å)	38.01 - 3.07
Number of reflections	47994
R_{work}/R_{free}	20.2/24.3
Number of atoms	
Protein	8901
Ligand/ion	15
Water	14
B-factors	
Protein	92.5
Ligand/ion	106.5
Water	61.1
RMS deviations	
Bond length (Å)	0.007
Bond angle (°)	1.279

*Highest-resolution shell is shown in parentheses.

The data for the Gas6/MYD1 crystal structure was collected from a single crystal.

Supplementary Table 6: Comparison of intermolecular contacts in wild-type Axl and MYD1 co-complexes

Gas6/wild-type Axl				
Hydrogen bonds†				
Res	wt Axl	Res	Gas6	Distance (Å)
48	ARG [NH2]	460	GLU [OE1]	3.3
56§	GLU [OE2]	308	ARG [NH1]	3.5
73	ASP [OD1]	314	LEU [N]	2.5
74	SER [N]	312	LYS [O]	3.1
74	SER [O]	313	ARG [NH2]	3.1
74	SER [O]	312	LYS [N]	3.0
75	THR [OG1]	313	ARG [NH2]	2.6
76	GLN [N]	310	ARG [O]	3.1
76	GLN [O]	310	ARG [N]	2.9
78	GLN [N]	308	ARG [O]	2.7
78	GLN [O]	308	ARG [N]	2.9
80	PRO [O]	299	ARG [NH2]	2.3
83	GLU [O]	302	SER [OG]	2.6
85	GLU [OE2]	304	THR [OG1]	2.9
Electrostatic interactions				
Res	wt Axl	Res.	Gas6	Distance (Å)
48	ARG [NH1]	460	GLU [OE1]	3.7
48	ARG [NH2]	460	GLU [OE1]	3.3
48	ARG [NH1]	460	GLU [OE2]	3.8
56	GLU [OE2]	308	ARG [NH1]	3.5
56	GLU [OE2]	308	ARG [NH2]	3.3
59§	GLU [OE1]	310	ARG [NH2]	3.5
59	GLU [OE2]	310	ARG [NH1]	3.4
59	GLU [OE2]	310	ARG [NE]	3.7
59	GLU [OE2]	310	ARG [NH2]	2.8
59	GLU [OE2]	312	LYS [NZ]	2.7

Gas6/MYD1				
Hydrogen bonds				
Res	MYD1	Res	Gas6	Distance (Å)
48	ARG [NH1]	456	THR [O]	3.2
56§	GLU [OE2]	308	ARG [NH2]	2.6
59	GLU [OE2]	312	LYS [NZ]	2.8
73	ASP [OD1]	314	LEU [N]	2.8
74	SER [N]	312	LYS [O]	3.0
74	SER [O]	313	ARG [NH2]	2.9
74	SER [O]	312	LYS [N]	3.0
75	THR [OG1]	313	ARG [NH2]	2.7
76	GLN [N]	310	ARG [O]	2.9
76	GLN [O]	310	ARG [N]	2.9
77	THR [OG1]	455	ASP [OD2]	3.1
78	GLN [N]	308	ARG [O]	2.7
78	GLN [O]	308	ARG [N]	2.9
78	GLN [OE1]	308	ARG [NH2]	2.9
80	PRO [O]	299	ARG [NH2]	2.3
83	GLU [O]	302	SER [OG]	2.8
Electrostatic interactions				
Res	MYD1	Res	Gas6	Distance (Å)
48	ARG [NH1]	460	GLU [OE1]	3.8
48	ARG [NH2]	460	GLU [OE1]	3.5
48	ARG [NH1]	460	GLU [OE2]	3.3
56	GLU [OE2]	308	ARG [NH1]	3.6
56	GLU [OE2]	308	ARG [NH2]	3.1
59§	GLU [OE1]	310	ARG [NH1]	3.7
59	GLU [OE2]	310	ARG [NH1]	2.9
59	GLU [OE2]	310	ARG [NE]	3.8
59	GLU [OE2]	310	ARG [NH2]	3.4
59	GLU [OE2]	312	LYS [NZ]	2.8

†Contacts common to both structures are grayed out in both lists.

§ Both R308 and R310 undergo significant conformational changes between the wild-type and MYD1 structures. While these two sets of interactions are technically identical from a crystallographic point of view, their structural changes were nonetheless important to note in **Supplementary Fig. 6a**.

Supplementary Table 7: Complete blood counts and chemistry panels for MYD1 Fc tolerability study

		MYD1 Fc			
Haematological	Carrier	1 mg/kg	10 mg/kg	Normal	Units
HCT	47 ± 0.7	38 ± 10.3	46 ± 0.8	39.0 - 47.0	%
RBC	9 ± 0.1	9 ± 0.0	8 ± 0.0	7.0 - 8.8	M/µl
HGB	15 ± 0.2	14 ± 0.1	14 ± 0.2	13.7 - 16.4	gm/dL
WBC	7 ± 1.0	4 ± 0.8	5 ± 1.9	5.5 - 9.3	k/µl
Platelet (estimate)	Adequate	Adequate	Adequate	Adequate	
Chemistry Panel					
Cholesterol	81 ± 1.5	28 ± 25.3	74 ± 1.8	N/A	mg/dL
Glucose	194 ± 3.5	200 ± 8.4	198 ± 22.6	184 - 220	mg/dL
Calcium	11 ± 0.1	11 ± 1.1	11 ± 0.1	8.9 - 9.7	mg/dL
Phosphorous	13 ± 0.6	12 ± 1.5	13 ± 1.1	N/A	mg/dL
Carbon dioxide	26 ± 1.1	22 ± 0.4	23 ± 2.2	N/A	mmol/L
Chloride	112 ± 2.6	124 ± 0.3	122 ± 2.7	N/A	mmol/L
Potassium	8 ± 0.4	8 ± 0.5	8 ± 0.9	3.0 - 9.6	mmol/L
Sodium	152 ± 4.6	156 ± 0.3	154 ± 2.1	114 - 154	mmol/L
Hepatic					
ALK	70 ± 17.9	83 ± 11.2	71 ± 15.5	76 - 160	U/L
AST	97 ± 18.3	136 ± 25.2	107 ± 20.4	192 - 388	U/L
ALP	106 ± 3.8	72 ± 34.7	79 ± 33.0	171 - 183	IU/L
Albumin	3.6 ± 0.0	3.3 ± 0.5	3.3 ± 0.5	3.2 - 3.6	g/dL
Protein (total)	6.1 ± 0.1	6.7 ± 0.3	6.4 ± 0.2	5.0 - 6.2	g/dL
Bilirubin (total)	0.1 ± 0.1	0.1 ± 0.1	0.1 ± 0.0	N/A	mg/dL
GGT	3 ± 2.1	1.7 ± 0.9	1.7 ± 0.3	N/A	U/L
Globulin	2.5 ± 0.1	3.3 ± 0.8	3.2 ± 0.4	N/A	
Renal					
BUN	23 ± 0.6	27 ± 0.9	23 ± 0.7	20.3 - 24.7	mg/dL
Creatinine	0.5 ± 0.3	0.5 ± 0.2	0.7 ± 0.0	0.1 - 1.1	mg/dL